

# Absence of a Relationship Between Surface Conductivity and Electrochemical Rates: Redox-Active Monolayers on Si(211), Si(111), and Si(110)

Song Zhang,<sup>a</sup> Stuart Ferrie,<sup>a</sup> Xin Lyu,<sup>a</sup> Yunfei Xia,<sup>b</sup> Nadim Darwish,<sup>a</sup> Zhenbo Wang,<sup>b</sup> Simone Ciampi<sup>a,\*</sup>

<sup>a</sup>School of Molecular and Life Sciences, Curtin University, Bentley, Western Australia 6102, Australia

<sup>b</sup>MIT Key Laboratory of Critical Materials Technology for New Energy Conversion and Storage, State Key Lab of Urban Water Resources and Environment, School of Chemistry and Chemical Engineering, Harbin Institute of Technology, Harbin 150001, China

---

**ABSTRACT:** Optimizing the kinetics of an electrode reaction is central to the design of devices whose function spans from sensing to energy conversion. Electrode kinetics depends strongly on electrode surface properties, but the search for optimal materials is often a trial-and-error process. Recent research has revealed a pronounced facet-dependent electrical conductivity for silicon, implicitly suggesting that rarely used crystallographic cuts of this technologically relevant material had been entirely overlooked for the fabrication of electrodes. By first protecting silicon from anodic decomposition through Si-C-bound organic monolayers, conductive atomic force microscopy demonstrates that conductivity decreases in the order (211) >> (110) > (111). However, charge-transfer rates for a model electrochemical reaction are similar on all these crystal orientations. These findings reveal the absence of a relationship between surface conductivity and kinetics of a surface confined redox reaction, and expand the range of silicon crystallographic orientations viable as electrode material.

---

## INTRODUCTION

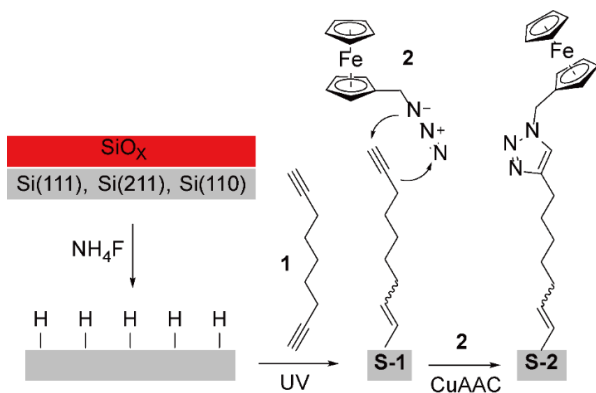
Starting from the seminal work of Sagiv in 1980,<sup>1</sup> fundamental and applied research on self-assembly of organic molecules onto electrode surfaces has continued gaining momentum.<sup>2</sup> While to date most of the research on self-assembly has focused on gold surfaces by exploiting alkanethiol chemistry,<sup>3</sup> the 1990s reports by Chidsey and co-workers of Si-C-bound monolayers helped to expand this research from metals to semiconductors.<sup>4-10</sup> Silicon remains the technologically most relevant semiconducting material,<sup>11-15</sup> and silicon electrodes that are functionalized with organic monolayers have broad application prospect in the fields of microscopy,<sup>16-17</sup> sensing,<sup>18-21</sup> chemical catalysis,<sup>22</sup> (bio)molecular electronics,<sup>6, 23-24</sup> and information storage.<sup>2, 25-26</sup>

Scientists and engineers working with silicon electrodes routinely rely on dynamic electrochemical measurements – principally cyclic voltammetry<sup>27</sup> – to extract kinetic information on electrode reactions.<sup>28-29</sup> But published data of redox kinetics on silicon are highly scattered.<sup>2</sup> Some of the experimental factors contributing to this irreproducibility issue are known,<sup>30</sup> others less so. Firstly, it is now generally agreed that common mathematical models used in the kinetic analysis of electrochemical data fall short of capturing all important descriptors of an electrified interface.<sup>29-32</sup> Secondly, minor changes to surface coverage of the redox molecule,<sup>33</sup> monolayer order<sup>34</sup> and intermolecular interactions<sup>32, 35</sup> are known to have dramatic kinetic effects.<sup>32, 36-37</sup> It remains less clear to what extent the chemical nature of the

interfacial bond – between organic monolayer and electrode – affects rates of surface-confined electrochemical reactions.<sup>38-39</sup> An important step in the direction of clarifying on this overlooked factor was recently published. Darwish and co-workers reported that for monolayers grafted on either indium-tin oxide (ITO), silicon or carbon electrodes there is a link between changes in molecular conductivities – ascribed unambiguously to different interfacial bonds – and differences in electrochemical rates.<sup>40</sup>

The origin of a putative link between electrical conductivity and electrochemical rates still lacks a conclusive explanation,<sup>39</sup> but its existence and manifestation would have immediate implications in silicon electrochemistry applied to sensing and catalysis. This is because an atomically flat silicon electrode is an idealization, and even well-prepared surfaces are a continuum of flat terraces separated by small vertical steps.<sup>9, 29, 41</sup> As a result, a silicon electrode of a given nominal orientation, such as commonly used Si(111) substrates, will inevitably expose a range of crystal facets, such as Si(110) and Si(211), of different surface conductivity. For example, data from Huang and co-workers indicate that the conductivity of silicon surfaces, measured with microscopic tungsten probes, decrease in the order (211)>>(111),<sup>42</sup> platinum-silicon junctions are more conductive when made on Si(110) rather than on Si(111),<sup>8</sup> and similar trends of facet-dependent conductivity have been reported for polyhedral Cu<sub>2</sub>O particles.<sup>43</sup>

The purpose of this paper is to clarify the presence or absence of a relationship between surface conductivity and electrochemical rates on oxide-free silicon electrodes. This is important since, to date, the vast majority of monolayer



**Scheme 1.** Preparation of hydrogen-terminated silicon electrodes on Si(111), Si(211), and Si(110), followed by UV-assisted hydrosilylation of 1,8-nonadiyne (**1**) to yield an alkyne-terminated silicon surface (**S-1**). Covalent grafting on **S-1** of azidomethylferrocene (**2**) via CuAAC “click” reactions generated a redox-active monolayer (**S-2**).

research on silicon has focused on Si(111) and Si(100) substrates,<sup>44-47</sup> and highly conductive crystal facets such as Si(110) and Si(211), which are readily available, have been entirely overlooked as potential electrode material.

## METHODS

**Silicon surface modification.** Unless otherwise specified, all chemical reagents were of analytical grade and used as received. Aqueous hydrogen peroxide solution (30 wt % in water, Sigma-Aldrich), sulfuric acid (Puranal, 95–97%, Sigma-Aldrich), and aqueous ammonium fluoride (40 wt%, Sigma-Aldrich) were of semiconductor grade. Redistilled solvents and Milli-Q™ water (>18 MΩ cm) were used for substrate cleaning procedures and to prepare electrolytic solutions. Azidomethylferrocene (**2**) was synthesized following literature procedures.<sup>48</sup> Boron-doped (0.007–0.013 Ω cm), 500–550 μm thick, prime-grade and single-side polished Si(111), Si(110), and Si(211) wafers (Czochralski process, <111>±0.5°, <110>±0.5°, <211>±0.5°) were purchased from Siltronix S.A.S. (Archamps, France). Prior to monolayer assembly (Scheme 1), silicon samples were cut into squares of 1 × 1 cm, and rinsed sequentially with dichloromethane, isopropanol and water. The samples were then immersed for 20 min in hot piranha solution (100 °C, the solution is a 3:1 mixture (v/v) of concentrated sulfuric acid (95–97%) and hydrogen peroxide (30%)), then washed with water and immediately transferred to a degassed etching solution of 40% ammonium fluoride (the solution was degassed by means of a 30 min argon bubbling). A trace amount of ammonium sulphite was added to the fluoride solution as an oxygen scavenger, and after nine minutes in the etching bath the hydrogen-terminated wafers were rinsed with copious water, dichloromethane, and then immediately reacted with a degassed sample of 1,8-nonadiyne. The liquid sample of 1,8-nonadiyne (**1**, ~50 μl) was then dropped on the silicon surface, and the

wet sample rested for two hours under UV light under nitrogen atmosphere. The source of 312 nm UV radiation (Vilber, VL-215.M, nominal power output of 30 W) was placed approximately 20 cm away from the sample.<sup>29</sup> Alkyne-terminated silicon samples (**S-1**) were then rinsed with isopropanol and kept under dichloromethane in a sealed reaction vial until analyzed or further reacted. Covalent attachment of azidomethylferrocene (**2**) on **S-1** surfaces followed a previously reported procedure.<sup>29</sup> In brief, to a sample vial containing the alkyne-terminated substrate sample (**S-1**), were added 5 mL of a 0.5 mM solution of **2** in an isopropanol and water mixture (1:1, v/v), copper(II) sulphate pentahydrate (20 mol% relative to the azide), and sodium ascorbate (ca. 100 mol% relative to the azide). The copper(I)-catalyzed azide-alkyne cycloaddition (CuAAC) reaction was carried out at room temperature, shielded from ambient light. After 40 min the reaction was quenched by removing the ferrocene-modified electrode (**S-2**) from the sample vial. The samples were rinsed with copious isopropanol, water, aqueous hydrochloric acid (0.5 M), water, isopropanol, dichloromethane, and then blown dry under nitrogen before analysis.

**Electrochemical measurements.** Cyclic voltammetry (CV) was performed on a CHI650D electrochemical workstation (CH Instruments, Austin, TX) using a three-electrode and single-compartment polytetrafluoroethylene (PTFE) custom cell. The modified silicon substrate served as the working electrode, a platinum mesh as the counter electrode, and an Ag/AgCl, 3.0 M aqueous NaCl, as the reference electrode. All electrochemical measurements were performed in aqueous 1.0 M perchloric acid (HClO<sub>4</sub>), in air at room temperature (22 ± 2 °C) and under dark inside a light-proof and grounded Faraday cage. All potentials are reported against the reference electrode. A circular Viton gasket defined the geometric area of the working electrode to 0.28 cm<sup>2</sup>, and ohmic contact between the back of the silicon sample and a copper plate was achieved by gently scribing the back of the electrode with emery paper before applying on it a small amount of gallium–indium eutectic. Surface coverages ( $\Gamma$ ) of ferrocene molecules are reported in mol cm<sup>-2</sup> and calculated from the Faradaic charge taken as the background-subtracted integrated current from the anodic scan of the voltammograms. A minimum of seven independently prepared samples was analyzed. The 99% confidence limit of the mean  $\Gamma$  was calculated as  $t_{n-1}s/n^{1/2}$ , where  $t_{n-1}$  is 3.71,  $s$  is the standard deviation, and  $n$  the number of measurements.<sup>49</sup> The apparent electron-transfer rate constants,  $k_{et}$ , for the electron-transfer reaction between tethered ferrocenes and the substrate was estimated from electrochemical impedance spectroscopy (EIS) measurements following the formalism developed by Laviron.<sup>50-51</sup> EIS data were collected between 10<sup>5</sup> Hz and 10<sup>-1</sup> Hz, and both the in-phase ( $Z'$ ) and out-of-phase impedance ( $Z''$ ) were extracted at the same time from the data and analyzed with the ZView and ZPlot software (Scribner Associates, Inc.). The  $k_{et}$  was calculated as  $1/(2 R_{ct}C_{ads})$ .<sup>50</sup> All EIS data were obtained at an applied working electrode DC potential,  $E_{dc}$ , equal to  $E_{1/2}$  ( $E_{1/2}$  is the mid-point between the potential of the anodic and cathodic CV current peaks), and by setting the potential amplitude of the AC perturbation to 15 mV. Samples for EIS measurements were prepared in quadruplicates and first analyzed by three consecutive CV cycles to estimate  $E_{1/2}$ .

The 99% confidence limit of the mean  $k_{\text{et}}$  was calculated as  $t_{n-1S}/n^{1/2}$ , with  $t_{n-1}$  set to 5.84.<sup>49</sup>

**Surface topography and electrical measurements.** Both topography and electrical conductivity data for monolayer-modified silicon samples were obtained by atomic force microscopy (AFM), in air and at room temperature. Topography measurements were conducted on a Park NX10 atomic force microscope operated in tapping mode. The topography data were analyzed with XEI software (Park Systems Corp.). The scan area was set to  $2 \times 2 \mu\text{m}$ , the resolution to 256 points/line, and the scan rate to 1.0 Hz. Antimony (n) doped silicon AFM tips (TESPAV2-Bruker) with spring constant of 42 N/m and resonance frequency of 320 kHz were used for the measurements. The electrical AFM experiments were conducted on a Bruker Dimension microscope with platinum AFM tips from Rocky Mountain Nanotechnology (25Pt300B, spring constant of  $18 \text{ N m}^{-1}$ ). The Bruker Peak Force Tunneling AFM (PF-TUNA) module was used to acquire current–voltage (I–V) data. I–V curves were acquired with the peak force set to  $2.5 \mu\text{N}$ , a current gain of either 10 nA/V or 100 nA/V, and a voltage sweep rate of 8.26 V/s. On each sample, individual I–V curves were sampled at 100 evenly spaced points, and a minimum of four samples for each silicon orientation was prepared and analyzed. All electrical AFM data were analyzed with Nano Scope 1.9.

**X-ray diffraction measurements (XRD).** XRD patterns were acquired on hydrogen-terminated silicon samples using a Bruker D2 PHASER X-ray diffractometer using a Cu  $K\alpha$  X-ray source ( $\lambda = 1.54 \text{ \AA}$ ).

**X-ray photoelectron spectroscopy (XPS).** XPS surface analysis was conducted using monochromatic Al  $K\alpha$  radiation with an Axis Supra (Kratos Analytical Ltd) instrument at 225 W. The instrument work function was calibrated to give a binding energy (BE) of 83.96 eV for the  $4f_{7/2}$  core level of gold, and the spectrometer dispersion was adjusted to give a BE of 932.62 eV for the  $2p_{3/2}$  core level of copper. The pass energy was set to 160 eV for survey spectra and 20 eV for high resolution spectra. All measurements were acquired in a hybrid lens mode which covers an analysis area of  $210000 \mu\text{m}^2$  ( $700 \times 300 \mu\text{m}$ ). Spectra were charge corrected to bring the main line of the C 1s core level spectrum to 285.0 eV.

## RESULTS AND DISCUSSION

All silicon samples in this work were hydrogen-terminated surfaces<sup>52</sup> modified by a hydrosilylation reaction (**1**,

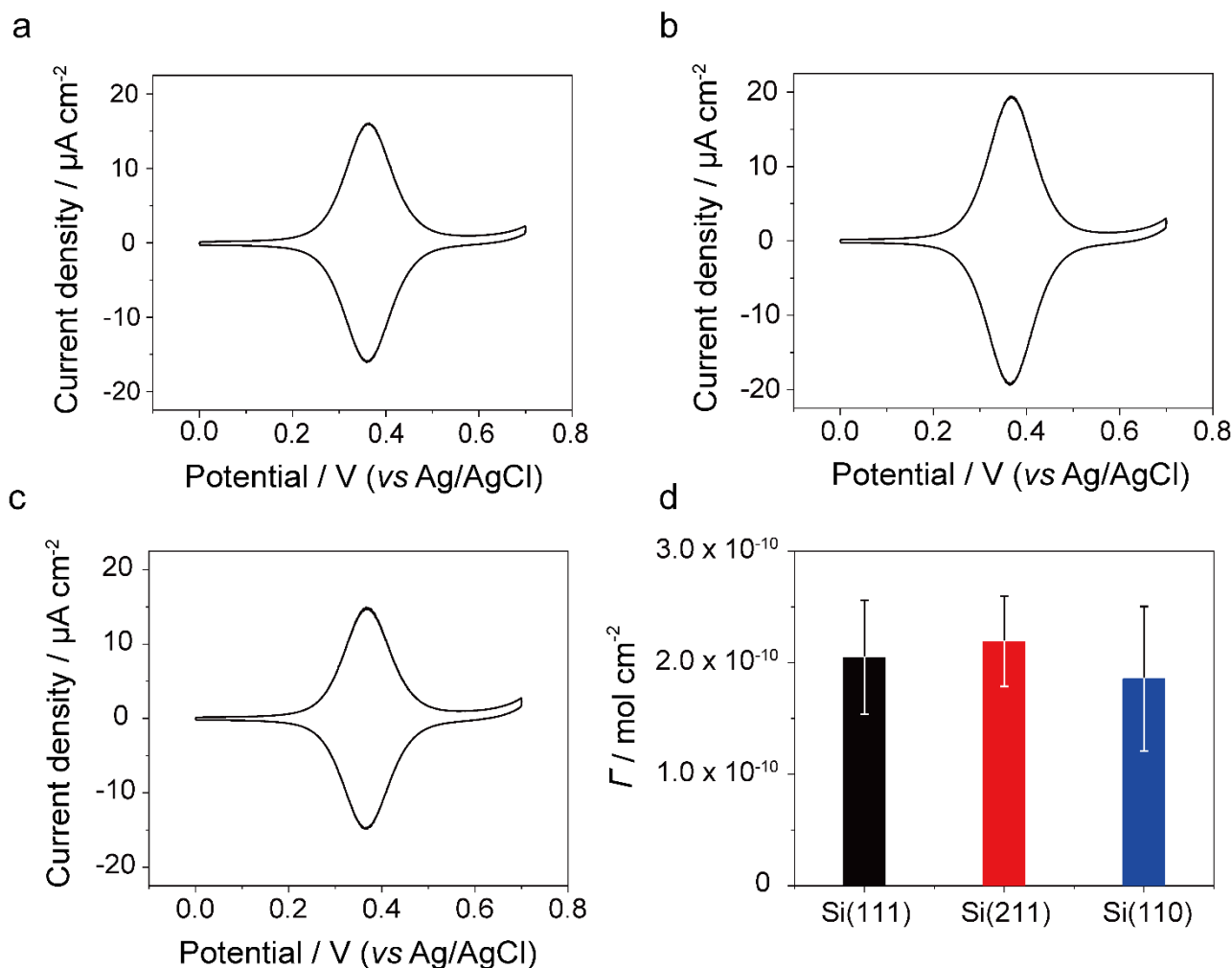


**Figure 1.** Representative cyclic voltammograms (CVs) for ferrocene monolayers (**S-2**) prepared on silicon substrates of different crystalline orientation ((a), Si(111); (b), Si(211); (c), Si(110)). The potential sweep started at 0 V (cathodic vertex). The voltage scan rate was 0.1 V/s, and the electrolyte aqueous 1.0 M HClO<sub>4</sub>. (d) CV-derived surface ferrocene coverage ( $\Gamma$ ) for **S-2** samples prepared on Si(111), Si(211) and Si(110) electrodes. Error bars indicate the 99% confidence limit of the mean.

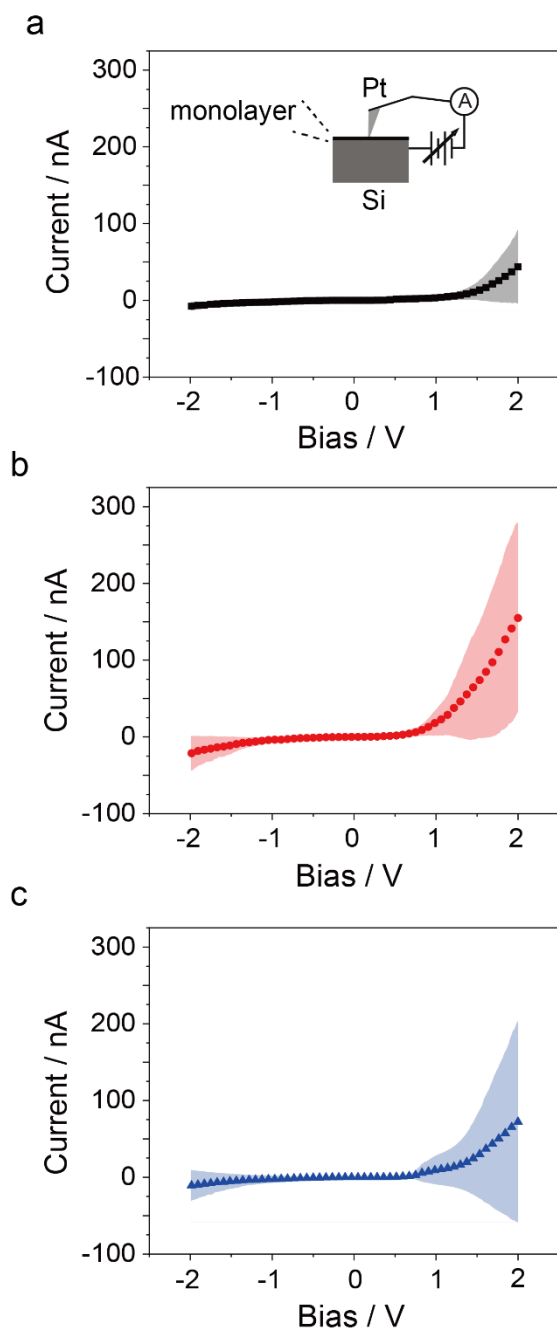


**Figure 2.** Measurement schematic and current-potential (I-V) data for platinum-silicon junctions obtained by conductive mode (PF-TUNA) atomic force microscopy (AFM) on monolayer-modified (**S-1**) Si(111) (a), Si(211) (b), and Si(110) (c). Solid symbols indicate the mean value of 400 I-V sweeps obtained on four independently prepared and analyzed samples. The colour-shaded areas represent the data standard deviation.

Scheme 1) to form a silicon-carbon-bound monolayer that minimizes anodic damaging of the substrate.<sup>48</sup> X-Ray diffraction (XRD) patterns are shown in Figure S1 (Supporting Information) and a stereographic projection indicating the relative orientation of the three crystal facets is in Figure S2. High-resolution X-ray photoelectron spectroscopy (XPS)

scans of the Si 2p region (Figure S3, Supporting Information) demonstrates the monolayer ability (**S-1**) to prevent appreciable oxidation of the underlying silicon substrate. XPS data indicate that for all three facets the amount of silicon oxide was below the spectrometer detection limit, and the deconvolution of the C 1s XPS narrow region (Figure S3) showed spectral features analogous 1-alkynes monolayers prepared on either H-Si(111) or H-Si(100) surfaces.<sup>53</sup>

The acetylene functionality of **S-1** samples allows tethering a redox-active molecule, and as shown in Scheme 1, ferrocene units (**2**) were grafted on the electrodes via a copper(I)-catalyzed azide-alkyne cycloaddition (CuAAC) reaction.<sup>54-55</sup> As the rate constant for a redox reaction involving a surface-bound redox molecule depends on the molecule surface density,<sup>33</sup> it was important to ensure a consistent ferrocene coverage before attempting a comparison between samples prepared on different silicon facets. Cyclic voltammetry (CV) experiments were therefore conducted to establish yields of the CuAAC reaction leading to **S-2**. Representative CVs are shown in Figure 1a-c, with a coverage analysis shown in Figure 1d. Coverages calculated from the Faradaic charge, taken as the background-subtracted integrated current from the anodic scan, are comparable on Si(111), Si(211), and Si(110), being  $(2.05 \pm 0.51) \times 10^{-10}$ ,  $(2.19 \pm 0.40) \times 10^{-10}$ , and  $(1.86 \pm 0.65) \times 10^{-10}$  mol cm<sup>-2</sup>, respectively. It is therefore unlikely that unequal surface coverages would lead to differences in  $k_{\text{et}}$  values, if any, between these three surface systems. This coverage is approximately 50% of that expected for a hexagonally close-packed full monolayer of ferrocene molecules, if the ferrocene molecules are assumed to be spherical with a diameter of 0.66 nm.<sup>56</sup>

Further, the ferrocene films exhibit CV waves with full width at half maximum (FWHM hereafter) of  $113 \pm 2$  mV in all the three substrates. The ideal fwhm from the Langmuir isotherm of a Nernstian process is 90.6 mV, and theoretical models are available to explain a non-ideal FWHM as a consequence of attractive/repulsive interactions experienced by the surface-tethered molecule.<sup>29</sup> FWHMs larger than 90.6 mV are often reported in literature<sup>57</sup> and can be explained as repulsive interactions between the electroactive species.<sup>30</sup> The magnitude of these unavoidable interactions is therefore comparable in all three surface systems. Electrostatic attractive forces between the positive ferricenium tethers and the substrate, which would manifest as a FWHM < 90.6 mV,<sup>29</sup> were not observed as prevented by the choice of highly doped p-type substrates.

Next the electrical conductivity of the Si(211), Si(111) and Si(100) surfaces were probed by conductive atomic force microscopy (cAFM, PF-TUNA) using solid platinum AFM tips as the top metal contact. Current-voltage measurements (I-Vs) of the platinum-monolayer-silicon junctions (**S-1** samples) are shown in Figure 2, and the bias routing is from the substrate to the tip, so that the forward current of the junction appears in the positive quadrant (positive current, positive bias). The I-V characteristics indicate that, regardless of the bias magnitude, the electrical junction conductivity is considerably larger on Si(211) than on Si(110), and that the least conductive systems are those

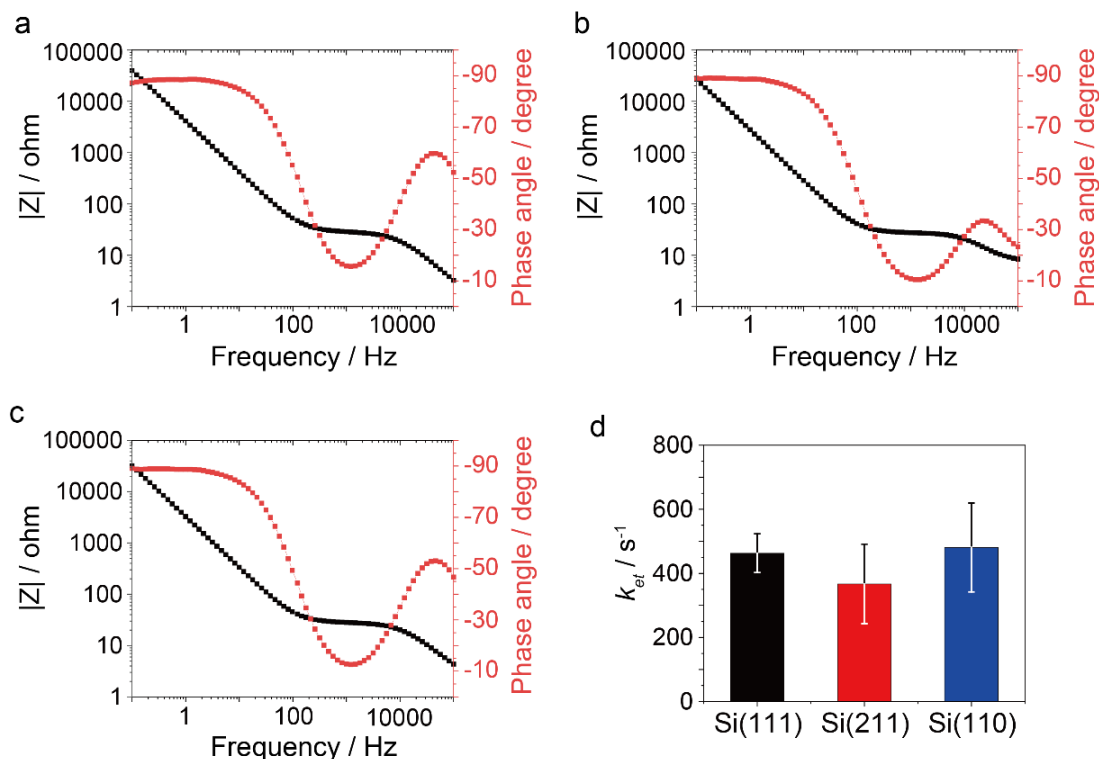


**Figure 3.** Representative EIS Bode plots for **S-2** samples prepared on silicon crystals of different orientation ((a), Si(111); (b), Si(211); (c) Si(110)). The DC bias of the EIS measurement was set to the  $E_{1/2}$  value obtained from CV measurements, and the amplitude of the AC perturbation was set to 15 mV. All experiments were performed in aqueous 1.0 M HClO<sub>4</sub>. (d) Plot of the EIS-derived  $k_{et}$  values. Error bars indicate the 99% confidence limit of the mean.

prepared on Si(111) crystals. For instance at a positive sample-tip bias of 1500 mV, which is approximately 300 mV more positive than the system flat-band potential (approximated as the bias at which forward currents begin to rise exponentially), the mean relative conductivities of Si(211), Si(110), and Si(111) are in the ratio 5.9:2.3:1.0. These mean conductivities are statistically different, as inferred by an independent samples *t*-test. For example comparing Si(211) against Si(111), the experimental *t* value at 1500 mV is 7.22, which is significantly greater than the critical *t* value of 2.58 (99% confidence).<sup>49</sup>

Measuring impedances over a broad range of frequencies allows to estimate individual element of an electrical circuit that can model the kinetics of a redox reaction.<sup>33</sup> Representative electrochemical impedance spectroscopy (EIS) data, obtained on **S-2** samples with the aim to estimate differences in  $k_{et}$  between Si(111), Si(211) and Si(110) are shown in Figure 3a–c. EIS data are displayed as Bode plots, which can visually highlight variations in electrochemical kinetics. As the AC frequency becomes comparable to the time constant of the redox reaction, the slope of  $Z$  vs frequency plot moves towards zero, and simultaneously the value of phase angle reaches its minimum. From the EIS plots in Figure 3 it is apparent that the three surface systems have very similar redox kinetics. A more detailed and quantitative treatment of the kinetic properties of **S-2** samples relied on an established formalism that describes the relationship between circuit elements ( $C_{ads}$ , adsorption pseudo-capacitance;  $R_{ct}$ , charge-transfer resistance; shown

in the equivalent circuit of Figure S4, Supporting Information) and the kinetic parameters of strongly adsorbed redox species.<sup>58–60</sup>  $C_{ads}$ , as well as the double-layer capacitance ( $C_{dl}$ ), showed frequency-dependent behavior and were therefore treated as constant-phase elements (CPEs). A CPE defines an inhomogeneity in the electrochemical system, such as kinetic dispersion.<sup>61</sup> However, in our redox monolayer systems the CPEs behave very similar to a capacitor, as the power-law modifiers have values between 0.95 and 0.99, where unity indicates an ideal capacitor. From the refined  $C_{ads}$  and  $R_{ct}$  values, electron-transfer rate constants,  $k_{et}$ , were estimated as  $(4.63 \pm 0.65) \times 10^2 \text{ s}^{-1}$  for Si(111),  $(3.67 \pm 1.24) \times 10^2 \text{ s}^{-1}$  for Si(211) and  $(4.81 \pm 1.38) \times 10^2 \text{ s}^{-1}$  for Si(110), therefore indistinguishable within the experimental error (Figure 3d). Further, for all the three systems, at low frequencies – where the impedance is dominated by double layer charging – the phase angle approaches  $-90^\circ$ , indicating that all samples are extremely smooth. The sigmoid shape that starts near  $0^\circ$  at high frequency and shifts close to  $-90^\circ$  at low frequencies is often diagnostic of monolayer imperfections and surface roughness, but in our experiments a minor dispersion is only observed for the more commonly used Si(111). The EIS-inferred superior smoothness of both Si(211) and Si(110) agrees with AFM topographic data (Figure S5, Supporting Information). This is an important finding, as it suggests that high quality monolayers can be prepared on a range of previously neglected low indexes silicon facets, such as Si(110) and Si(211).

## CONCLUSIONS

We have explored a model electrochemical reaction, the oxidation and reduction of ferrocene, in diffusionless monolayer systems prepared on Si(111), Si(211) and Si(110) surfaces. In all three cases the redox system behaves close to ideality, suggesting that highly conductive (211) and (110) silicon crystals are an excellent alternative to conventional and widespread Si(111) substrates. Current–potential characteristics acquired by conductive atomic force microscopy reveals that surface conductivity decreases in the order Si(211)>>Si(110)>Si(111). Unlike systems where differences in electrical conductivity are imparted by changes to the chemical nature of the monolayer anchoring group,<sup>40</sup> and unlike the inverse relationship between electron transfer rate constants and the length of alkyl spacers separating electrode and redox unit,<sup>62–63</sup> we found that identical surface chemistry on Si(211), Si(110), and Si(111) leads to comparable kinetics of a redox reaction occurring at the monolayer distal end. While other higher index substrates, such as Si(311) and Si(411), remain to be investigated, the current findings demonstrate a pronounced facet-dependent electrical conductivity,<sup>64</sup> expand the range of silicon orientations viable as electrode material, and suggest literature discrepancies in electrochemical rate constants not to be linked to substrate defects, such as ubiquitous surface miscuts.

## ASSOCIATED CONTENT

Additional AFM, XPS, and XRD data, EIS model. This material is available free of charge via the Internet at <http://pubs.acs.org>.

## AUTHOR INFORMATION

### Corresponding Author

**Simone Ciampi** – School of Molecular and Life Sciences, Curtin University, Bentley, Western Australia 6102, Australia; [orcid.org/0000-0002-8272-8454](https://orcid.org/0000-0002-8272-8454); Email: [simone.ciampi@curtin.edu.au](mailto:simone.ciampi@curtin.edu.au)

### Authors

**Song Zhang** – School of Molecular and Life Sciences, Curtin University, Bentley, Western Australia 6102, Australia; [orcid.org/0000-0002-3387-4957](https://orcid.org/0000-0002-3387-4957)

**Stuart Ferrie** – School of Molecular and Life Sciences, Curtin University, Bentley, Western Australia 6102, Australia; [orcid.org/0000-0001-8988-8293](https://orcid.org/0000-0001-8988-8293)

**Xin Lyu** – School of Molecular and Life Sciences, Curtin University, Bentley, Western Australia 6102, Australia; [orcid.org/0000-0002-6506-0392](https://orcid.org/0000-0002-6506-0392)

**Yunfei Xia** – MIIT Key Laboratory of Critical Materials Technology for New Energy Conversion and Storage, State Key Lab of Urban Water Resources and Environment, School of Chemistry and Chemical Engineering, Harbin Institute of Technology, Harbin 150001, China

**Nadim Darwish** – School of Molecular and Life Sciences, Curtin University, Bentley, Western Australia 6102, Australia; [orcid.org/0000-0002-6565-1723](https://orcid.org/0000-0002-6565-1723)

**Zhenbo Wang** – MIIT Key Laboratory of Critical Materials Technology for New Energy Conversion and Storage,

State Key Lab of Urban Water Resources and Environment, School of Chemistry and Chemical Engineering, Harbin Institute of Technology, Harbin 150001, China; [orcid.org/0000-0001-9388-1481](https://orcid.org/0000-0001-9388-1481)

## Notes

The authors declare no competing financial interest.

## ACKNOWLEDGMENTS

The authors acknowledge support from the Australian Research Council (DP190100735 and FT190100148). We thank A/Prof. Josh Lipton-Duffin (Queensland University of Technology) for the assistance with the XPS analysis.

## REFERENCES

- (1) Sagiv, J., Organized Monolayers by Adsorption. 1. Formation and Structure of Oleophobic Mixed Monolayers on Solid Surfaces. *J. Am. Chem. Soc.* **1980**, *102*, 92–98.
- (2) Fabre, B., Functionalization of Oxide-Free Silicon Surfaces with Redox-Active Assemblies. *Chem. Rev.* **2016**, *116*, 4808–4849.
- (3) Vericat, C.; Vela, M. E.; Benitez, G.; Carro, P.; Salvarezza, R. C., Self-Assembled Monolayers of Thiols and Dithiols on Gold: New Challenges for a Well-Known System. *Chem. Soc. Rev.* **2010**, *39*, 1805–1834.
- (4) Linford, M. R.; Chidsey, C. E. D., Alkyl Monolayers Covalently Bonded to Silicon Surfaces. *J. Am. Chem. Soc.* **1993**, *115*, 12631–12632.
- (5) Linford, M. R.; Fenter, P.; Eisenberger, P. M.; Chidsey, C. E. D., Alkyl Monolayers on Silicon Prepared from 1-Alkenes and Hydrogen-Terminated Silicon. *J. Am. Chem. Soc.* **1995**, *117*, 3145–3155.
- (6) Aragonès, A. C.; Darwish, N.; Ciampi, S.; Sanz, F.; Gooding, J. J.; Díez-Pérez, I., Single-Molecule Electrical Contacts on Silicon Electrodes under Ambient Conditions. *Nat. Commun.* **2017**, *8*, 15056.
- (7) Peiris, C. R.; Vogel, Y. B.; Le Brun, A. P.; Aragonès, A. C.; Coote, M. L.; Díez-Pérez, I.; Ciampi, S.; Darwish, N., Metal-Single-Molecule-Semiconductor Junctions Formed by a Radical Reaction Bridging Gold and Silicon Electrodes. *J. Am. Chem. Soc.* **2019**, *141*, 14788–14797.
- (8) Vasquez, R. M.; Hlynchuk, S.; Maldonado, S., Effect of Covalent Surface Functionalization of Si on the Activity of Trifluoromethanesulfonic Anhydride for Suppressing Surface Recombination. *ACS Appl. Mater. Interfaces* **2020**, *12*, 57560–57568.
- (9) Zhang, S.; Ferrie, S.; Peiris, C. R.; Lyu, X.; Vogel, Y. B.; Darwish, N.; Ciampi, S., Common Background Signals in Voltammograms of Crystalline Silicon Electrodes are Reversible Silica–Silicon Redox Chemistry at Highly Conductive Surface Sites. *J. Am. Chem. Soc.* **2021**, *143*, 1267–1272.
- (10) Downes, N.; Cheek, Q.; Maldonado, S., Electroreduction of Perchlorinated Silanes for Si Electrodeposition. *J. Electrochem. Soc.* **2021**, *168*, 022503.
- (11) Landman, U.; Barnett, R. N.; Scherbakov, A. G.; Avouris, P., Metal-Semiconductor Nanocontacts: Silicon Nanowires. *Phys. Rev. Lett.* **2000**, *85*, 1958–1961.
- (12) Schmehl, A.; Vaithyanathan, V.; Herrnberger, A.; Thiel, S.; Richter, C.; Liberati, M.; Heeg, T.; Ruckerath, M.; Kourkoutis, L. F.; Muhlbauer, S.; Boni, P.; Muller, D. A.; Barash, Y.; Schubert, J.; Idzerda, Y.; Mannhart, J.; Schlom, D. G., Epitaxial Integration of the Highly Spin-Polarized Ferromagnetic Semiconductor EuO with Silicon and GaN. *Nat. Mater.* **2007**, *6*, 882–887.
- (13) Zhang, H.; Liu, H.; Wei, K.; Kurakevych, O. O.; Le Godec, Y.; Liu, Z.; Martin, J.; Guerrette, M.; Nolas, G. S.; Strobel, T. A., BC8 Silicon (Si-III) is a Narrow-Gap Semiconductor. *Phys. Rev. Lett.* **2017**, *118*, 146601.
- (14) Lapano, J.; Brahlek, M.; Zhang, L.; Roth, J.; Pogrebnaykov, A.; Engel-Herbert, R., Scaling Growth Rates for Perovskite Oxide Virtual Substrates on Silicon. *Nat. Commun.* **2019**, *10*, 2464.
- (15) Wang, J.; Yang, Z.; Chen, W.; Du, L.; Jiao, B.; Krause, S.; Wang, P.; Wei, Q.; Zhang, D.-W.; Wu, C., Modulated Light-Activated Electrochemistry at Silicon Functionalized with Metal–Organic Frameworks Towards Addressable DNA Chips. *Biosens. Bioelectron.* **2019**, *146*, 111750.

- (16) Vogel, Y. B.; Darwish, N.; Ciampi, S., Spatiotemporal Control of Electrochemiluminescence Guided by a Visible Light Stimulus. *Cell Rep. Phys. Sci.* **2020**, *1*, 100107.
- (17) Ciampi, S.; James, M.; Le Saux, G.; Gaus, K.; Justin Gooding, J., Electrochemical "Switching" of Si(100) Modular Assemblies. *J. Am. Chem. Soc.* **2012**, *134*, 844–847.
- (18) Qin, G.; Santos, C.; Zhang, W.; Li, Y.; Kumar, A.; Erasquin, U. J.; Liu, K.; Muradov, P.; Trautner, B. W.; Cai, C., Biofunctionalization on Alkylated Silicon Substrate Surfaces via "Click" Chemistry. *J. Am. Chem. Soc.* **2010**, *132*, 16432–16441.
- (19) Chen, L.; Zhou, Y.; Jiang, S.; Kunze, J.; Schmuki, P.; Krause, S., High resolution LAPS and SPIM. *Electrochem. Commun.* **2010**, *12*, 758–760
- (20) Juan-Colás, J.; Parkin, A.; Dunn, K. E.; Scullion, M. G.; Krauss, T. F.; Johnson, S. D., The Electrophotonic Silicon Biosensor. *Nat. Commun.* **2016**, *7*, 12769.
- (21) Terrero Rodríguez, I. M.; Borrill, A. J.; Schäffer, K. J.; Hernandez, J. B.; O'Neil, G. D., Light-Addressable Electrochemical Sensing with Electrodeposited n-Silicon/Gold Nanoparticle Schottky Junctions. *Anal. Chem.* **2020**, *92*, 11444–11452.
- (22) Pekarek, R. T.; Kearney, K.; Simon, B. M.; Ertekin, E.; Rockett, A. A.; Rose, M. J., Identifying Charge Transfer Mechanisms across Semiconductor Heterostructures via Surface Dipole Modulation and Multiscale Modeling. *J. Am. Chem. Soc.* **2018**, *140*, 13223–13232.
- (23) Ciampi, S.; Gooding, J. J., Direct Electrochemistry of Cytochrome c at Modified Si(100) Electrodes. *Chem. Eur. J.* **2010**, *16*, 5961–5968.
- (24) Chen, X.; Park, Y. J.; Kang, M.; Kang, S.-K.; Koo, J.; Shinde, S. M.; Shin, J.; Jeon, S.; Park, G.; Yan, Y.; MacEwan, M. R.; Ray, W. Z.; Lee, K.-M.; Rogers, J. A.; Ahn, J.-H., CVD-grown monolayer MoS<sub>2</sub> in bioabsorbable electronics and biosensors. *Nat. Commun.* **2018**, *9*, 1690.
- (25) Fabre, B., Ferrocene-Terminated Monolayers Covalently Bound to Hydrogen-Terminated Silicon Surfaces. Toward the Development of Charge Storage and Communication Devices. *Acc. Chem. Res.* **2010**, *43*, 1509–1518.
- (26) Fabre, B.; Pujari, S. P.; Scheres, L.; Zuilhof, H., Micropatterned Ferrocenyl Monolayers Covalently Bound to Hydrogen-Terminated Silicon Surfaces: Effects of Pattern Size on the Cyclic Voltammetry and Capacitance Characteristics. *Langmuir* **2014**, *30*, 7235–7243.
- (27) Heinze, J., Cyclic Voltammetry—"Electrochemical Spectroscopy". New Analytical Methods (25). *Angew. Chem. Int. Ed.* **1984**, *23*, 831–847.
- (28) Santangelo, P. G.; Miskelly, G. M.; Lewis, N. S., Cyclic Voltammetry at Semiconductor Photoelectrodes. 1. Ideal Surface-Attached Redox Couples with Ideal Semiconductor Behavior. *J. Phys. Chem.* **1988**, *92*, 6359–6367.
- (29) Vogel, Y. B.; Zhang, L.; Darwish, N.; Gonçalves, V. R.; Le Brun, A.; Gooding, J. J.; Molina, A.; Wallace, G. G.; Coote, M. L.; Gonzalez, J.; Ciampi, S., Reproducible Flaws Unveil Electrostatic Aspects of Semiconductor Electrochemistry. *Nat. Commun.* **2017**, *8*, 2066.
- (30) Vogel, Y. B.; Molina, A.; Gonzalez, J.; Ciampi, S., Quantitative Analysis of Cyclic Voltammetry of Redox Monolayers Adsorbed on Semiconductors: Isolating Electrode Kinetics, Lateral Interactions, and Diode Currents. *Anal. Chem.* **2019**, *91*, 5929–5937.
- (31) Vogel, Y. B.; Molina, A.; Gonzalez, J.; Ciampi, S., Microelectrode Arrays with Active-Area Geometries Defined by Spatial Light Modulation. *Electrochim. Acta* **2020**, *356*, 136849.
- (32) Gonzalez, J.; Sequí-Castellano, J. A., Electrochemical Determination of Kinetic Parameters of Surface Confined Redox Probes in Presence of Intermolecular Interactions by Means of Cyclic Voltammetry. Application to TEMPO Monolayers in Gold and Platinum Electrodes. *Electrochim. Acta* **2021**, *365*, 137331.
- (33) Ciampi, S.; Choudhury, M. H.; Ahmad, S. A. B. A.; Darwish, N.; Brun, A. L.; Gooding, J. J., The Impact of Surface Coverage on the Kinetics of Electron Transfer Through Redox Monolayers on a Silicon Electrode Surface. *Electrochim. Acta* **2015**, *186*, 216–222.
- (34) Laborda, E.; González, J.; Molina, A., Analytical Theory for Ion Transfer-Electron Transfer Coupled Reactions at Redox Layer-Modified/Thick Film-Modified Electrodes. *Curr. Opin. Electrochem.* **2020**, *19*, 78–87.
- (35) Gonzalez, J.; Sequí, J.-A., Kinetic Implications of the Presence of Intermolecular Interactions in the Response of Binary Self-Assembled Electroactive Monolayers. *ACS Omega* **2018**, *3*, 1276–1292.
- (36) Dhar, D.; McKenas, C. G.; Huang, C.-W.; Atkin, J. M.; Dempsey, J. L.; Lockett, M. R., Quantitative Effects of Disorder on Chemically Modified Amorphous Carbon Electrodes. *ACS Appl. Energy Mater.* **2020**, *3*, 8038–8047.
- (37) Patel, D. A.; Chevalier, R. B.; Weller, A. M.; Shakespeare, C. C.; Soares, E. J.; Landis, E. C., Porosity Effects on the Ordering and Stability of Self-Assembled Monolayers on Nanoporous Gold. *J. Phys. Chem. C* **2020**, *124*, 26851–26863.
- (38) Chen, F.; Li, X.; Hihath, J.; Huang, Z.; Tao, N., Effect of Anchoring Groups on Single-Molecule Conductance: Comparative Study of Thiol-, Amine-, and Carboxylic-Acid-Terminated Molecules. *J. Am. Chem. Soc.* **2006**, *128*, 15874–15881.
- (39) Wierzbinski, E.; Venkatramani, R.; Davis, K. L.; Bezer, S.; Kong, J.; Xing, Y.; Borguet, E.; Achim, C.; Beratan, D. N.; Waldeck, D. H., The Single-Molecule Conductance and Electrochemical Electron-Transfer Rate Are Related by a Power Law. *ACS Nano* **2013**, *7*, 5391–5401.
- (40) Dief, E. M.; Darwish, N., Ultrasonic Generation of Thiyl Radicals: A General Method of Rapidly Connecting Molecules to a Range of Electrodes for Electrochemical and Molecular Electronics Applications. *ACS Sens.* **2021**, *6*, 573–580.
- (41) Allongue, P.; Henry de Villeneuve, C.; Morin, S.; Boukherroub, R.; Wayner, D. D. M., The Preparation of Flat H-Si(111) Surfaces in 40% NH<sub>4</sub>F Revisited. *Electrochim. Acta* **2000**, *45*, 4591–4598.
- (42) Tan, C.-S.; Hsieh, P.-L.; Chen, L.-J.; Huang, M. H., Silicon Wafers with Facet-Dependent Electrical Conductivity Properties. *Angew. Chem. Int. Ed.* **2017**, *56*, 15339–15343.
- (43) Vogel, Y. B.; Zhang, J.; Darwish, N.; Ciampi, S., Switching of Current Rectification Ratios within a Single Nanocrystal by Facet-Resolved Electrical Wiring. *ACS Nano* **2018**, *12*, 8071–8080.
- (44) Rohde, R. D.; Agnew, H. D.; Yeo, W.-S.; Bailey, R. C.; Heath, J. R., A Non-Oxidative Approach toward Chemically and Electrochemically Functionalizing Si(111). *J. Am. Chem. Soc.* **2006**, *128*, 9518–9525.
- (45) O'Leary, L. E.; Rose, M. J.; Ding, T. X.; Johansson, E.; Brunschwig, B. S.; Lewis, N. S., Heck Coupling of Olefins to Mixed Methyl/Thienyl Monolayers on Si(111) Surfaces. *J. Am. Chem. Soc.* **2013**, *135*, 10081–10090.
- (46) Zhang, L.; Vogel, Y. B.; Noble, B. B.; Goncales, V. R.; Darwish, N.; Brun, A. L.; Gooding, J. J.; Wallace, G. G.; Coote, M. L.; Ciampi, S., TEMPO Monolayers on Si(100) Electrodes: Electrostatic Effects by the Electrolyte and Semiconductor Space-Charge on the Electroactivity of a Persistent Radical. *J. Am. Chem. Soc.* **2016**, *138*, 9611–9619.
- (47) Yang, Y.; Ciampi, S.; Gooding, J. J., Coupled Thermodynamic and Kinetic Changes in the Electrochemistry of Ferrocenyl Monolayers Induced by Light. *Langmuir* **2017**, *33*, 2497–2503.
- (48) Ciampi, S.; Eggers, P. K.; Le Saux, G.; James, M.; Harper, J. B.; Gooding, J. J., Silicon (100) electrodes resistant to oxidation in aqueous solutions: an unexpected benefit of surface acetylene moieties. *Langmuir* **2009**, *25*, 2530–2539.
- (49) Miller, J. N.; Miller, J. C., *Statistics and Chemometrics for Analytical Chemistry*. 5th ed. Pearson education: Essex, England, 2005.
- (50) Laviron, E., Surface linear potential sweep voltammetry: Equation of the peaks for a reversible reaction when interactions between the adsorbed molecules are taken into account. *J. Electroanal. Chem. Interf. Electrochem.* **1974**, *52*, 395–402.
- (51) Laviron, E., The use of linear potential sweep voltammetry and of a.c. voltammetry for the study of the surface electrochemical reaction of strongly adsorbed systems and of redox modified electrodes. *J. Electroanal. Chem.* **1979**, *100*, 263–270.
- (52) Higashi, G. S.; Becker, R. S.; Chabal, Y. J.; Becker, A. J., Comparison of Si(111) Surfaces Prepared Using Aqueous Solutions of NH<sub>4</sub>F versus HF. *Appl. Phys. Lett.* **1991**, *58*, 1656–1658.
- (53) Kondo, M.; Mates, T. E.; Fischer, D. A.; Wudl, F.; Kramer, E. J., Bonding Structure of Phenylacetylene on Hydrogen-Terminated Si(111) and Si(100): Surface Photoelectron Spectroscopy Analysis and Ab Initio Calculations. *Langmuir* **2010**, *26*, 17000–17012.
- (54) Ciampi, S.; Bocking, T.; Kilian, K. A.; James, M.; Harper, J. B.; Gooding, J. J., Functionalization of Acetylene-Terminated Monolayers on Si(100) Surfaces: A Click Chemistry Approach. *Langmuir* **2007**, *23*, 9320–9329.
- (55) Ciampi, S.; Harper, J. B.; Gooding, J. J., Wet Chemical Routes to the Assembly of Organic Monolayers on Silicon Surfaces via the Formation of Si-C Bonds: Surface Preparation, Passivation and Functionalization. *Chem. Soc. Rev.* **2010**, *39*, 2158–2183.
- (56) Rowe, G. K.; Creager, S. E., Redox and Ion-Pairing Thermodynamics in Self-Assembled Monolayers. *Langmuir* **1991**, *7*, 2307–2312.

- (57) Paxton, W. F.; Kleinman, S. L.; Basuray, A. N.; Stoddart, J. F.; Van Duyne, R. P., Surface-Enhanced Raman Spectroelectrochemistry of TTF-Modified Self-Assembled Monolayers. *J. Phys. Chem. Lett.* **2011**, *2*, 1145–1149.
- (58) Laviron, E., A.C. Polarography and Faradaic Impedance of Strongly Adsorbed Electroactive Species: Part I. Theoretical and Experimental Study of a Quasi-Reversible Reaction in the Case of a Langmuir Isotherm. *J. Electroanal. Chem. Interf. Electrochem.* **1979**, *97*, 135–149.
- (59) Creager, S. E.; Wooster, T. T., A New Way of Using ac Voltammetry To Study Redox Kinetics in Electroactive Monolayers. *Anal. Chem.* **1998**, *70*, 4257–4263.
- (60) Abhayawardhana, A. D.; Sutherland, T. C., Heterogeneous Proton-Coupled Electron Transfer of an Aminoanthraquinone Self-Assembled Monolayer. *J. Phys. Chem. C* **2009**, *113*, 4915–4924.
- (61) Brevnov, D. A.; Finklea, H. O.; Van Ryswyk, H., AC Voltammetry Studies of Electron Transfer Kinetics for a Redox Couple Attached via Short Alkanethiols to a Gold Electrode. *J. Electroanal. Chem.* **2001**, *500*, 100–107.
- (62) Eckermann, A. L.; Feld, D. J.; Shaw, J. A.; Meade, T. J., Electrochemistry of Redox-Active Self-Assembled Monolayers. *Coord. Chem. Rev.* **2010**, *254*, 1769–1802.
- (63) Eggers, P. K.; Darwish, N.; Paddon-Row, M. N.; Gooding, J. J., Surface-Bound Molecular Rulers for Probing the Electrical Double Layer. *J. Am. Chem. Soc.* **2012**, *134*, 7539–7544.
- (64) Tan, C.-S.; Huang, M. H., Metal-like Band Structures of Ultrathin Si {111} and {112} Surface Layers Revealed through Density Functional Theory Calculations. *Chem. Eur. J.* **2017**, *23*, 11866–11871.

## TOC Graphic

